



Research Article

CFD modelling of the microclimate of a cultivated greenhouse: A validation study between experimental and numerical results

Soumaïla TIGAMPO^{1,*}, Sami KOOLI², Nizar Ben SALAH³, Walid FOU DHIL⁴,
Reda ERRAIS⁵, Vincent SAMBOU¹, Sadok Ben JABRALLAH⁴

¹Water, Energy, Environment and Industrial Processes Laboratory (LE3PI), Ecole Supérieure Polytechnique de Dakar of Cheikh Anta Diop University, Dakar-Fann, 5085, Senegal

²Research and Technology Center of Energy, Thermal Processes Laboratory, Hammam-Lif, Tunis, 1008, Tunisia

³Laboratory of Mechanics, Materials and Processes, Ecole Nationale Supérieure d'Ingénieur de Tunis, 1008, Tunisia

⁴Laboratory for Energy, Heat and Mass Transfer, Faculty of Sciences of Bizerte, University of Carthage, 1054, Tunisia

⁵Institute of Agronomy and Veterinary Hassan II, Rabat, Morocco

ARTICLE INFO

Article history

Received: 22 December, 2021

Accepted: 17 December, 2022

Keywords:

Ansys-Fluent; CFD Modelling; Validation; Greenhouse; Plant; Radiation Model (Discrete Ordinate)

ABSTRACT

In this work, we present the validation of a numerical model of a greenhouse thermally insulated on three sides with a tomato crop. A CFD software (Ansys-Fluent) was used to solve the numerical model. The discrete ordinate model was included to solve the radiative transfer equation. The results of the numerical model were compared with the values of air temperature observations at different points in the greenhouse. Good agreement was obtained between the simulated and measured values, with coefficients of determination $R^2 = 0.77$, $R^2 = 0.84$, $R^2 = 0.99$, and $R^2 = 0.89$ for the temperatures of the points 10 cm, 80 cm, and 210 cm above the ground and the average temperature in the greenhouse, respectively. A third-order polynomial curve was drawn between the simulated and measured values of relative humidity in the greenhouse. These R^2 values are 0.9786 and 0.7165, the simulated and measured relative humidity, respectively. The simulation results showed low velocity values with an average of 0.525 m/s located between 1.5 m and 2 m from the ground.

Cite this article as: Tigampo S, Kooli S, Salah NB, Foudhil W, Errais R, Sambou V, Jabrallah SB. CFD modelling of the microclimate of a cultivated greenhouse: A validation study between experimental and numerical results. J Ther Eng 2023;9(5):1115–1129.

INTRODUCTION

Nowadays, despite the access to technology, humanity faces severe problems in ensuring food supply to the population. This is why the amount of food produced would be shortly insufficient to meet the demand for food needs in the

world [1]. The shortfall in the food supply is partly related to climate change and the rapid growth of the world's population, which currently stands at 7.6 billion. It is expected to reach 9.8 billion by 2050 and 11.2 billion by 2100 [2]. The Food and Agriculture Organization of the United Nations

*Corresponding author.

*E-mail address: tigamposoumaila@gmail.com

This article has been recommended for publication in a revised form by Assigned Editor Ozgen Acikgoz



[3] estimates that 820 million people will not have enough to eat in 2018. In particular, the situation is relatively worrying in Africa. Indeed, it is the continent with the highest hunger rates globally. Solar greenhouses are an exciting solution in our countries to alleviate this problem of food imbalance. Solar energy is an exciting alternative to fossil fuels for greenhouse agricultural applications and contributes to reducing CO₂ emissions in nature. A well installed greenhouse provides a favourable environment in terms of relative humidity, temperature and air exchange, conducive to plant growth. In this way, production can be increased by creating a favourable microclimate for year-round cultivation using the greenhouse system method.

However, it is difficult to fully control the greenhouse microclimate because it depends on several external climatic factors (temperature, solar radiation, wind speed and direction) and the type of materials used to build the greenhouse [4, 5]. A good understanding of the thermal behaviour of greenhouses for efficient use is necessary. Its application integrates several fields such as agriculture, drying, aquaculture, soil solarisation and poultry. Its broadened scope has led to significant advances in research and development.

This paper studies the numerical modelling in three dimensions of a solar greenhouse with tomato crops. The aim is to perform a numerical validation of the experimental data. For this purpose, we will study the heat and mass transfers that occur in the greenhouse with tomato crops.

Bouadila et al. [6] studied two identical greenhouses, one of which has a 'CSASTL' latent heat storage air collector. Both greenhouses were planted with tomato plants during winter. The results showed that the temperature inside the greenhouse without the collector had maximum values between 25 and 45 °C, which exceeded the optimal operating temperature of the tomatoes, which varied between 20 and 30 °C. The daily variation of the air temperature inside the greenhouse without a sensor also exceeds the air temperature inside the greenhouse with "CSASTL", with a difference varying between 1 and 3.6 °C between 10:00 and 16:30. From 21:00 onwards, the sensor keeps the air temperature constant at around 12 °C throughout the night.

S. Kooli et al. [7] ont étudié l'effet d'un volet de nuit sur une serre isolée. Le premier dispose d'un système de chauffage solaire qui stocke l'énergie thermique pendant la journée et la restitue pendant la nuit. Les résultats expérimentaux ont montré que les variations nocturnes de la température de l'air à l'intérieur des deux serres étaient supérieures de 2°C entre la première (avec volet) et la seconde (sans volet). Mais aussi, la température de l'air à l'intérieur de la serre avec un système de chauffage a été maintenue à 15 °C tandis que la température de l'air extérieur était de 8 °C pendant la nuit.

M. Naseer et al. [8] conducted a bio-economic evaluation of greenhouse designs for seasonal tomato production in Norway. They identify one greenhouse design among several realised that generated the highest net financial return and lowest energy consumption for seasonal tomato

production. A model-based greenhouse design method, including modules for indoor greenhouse climate, crop growth, yield prediction and economics, was applied to predict net financial return and energy consumption. The highest financial return is 47.6 NOK m⁻² for the greenhouse design with a night energy screen.

Researchers have established several models based on heat budgets with systems of equations to predict the temperature, speed and rate of air exchange in the greenhouse [9–11].

G. Tonga et al. [12] state that these theoretical models developed to predict indoor air temperatures all assume uniform temperatures in the greenhouse. These techniques do not clearly map the physical quantities, giving a detailed picture of the temperature profiles and airflow field in the greenhouse. These temperature variations in each part of the greenhouse are highly dynamic processes in time and space and are not accurately modelled by these models. On the other hand, fluid dynamics (CFD) modelling is considered a powerful technique to simulate the time and space-dependent microclimate of the greenhouse.

This tool has enabled progress to be made in the simulation studies of heat and mass transfers, airspeed, air humidity and even the layout of openings. Thus, there are several works that have been brought in a closed greenhouse, a naturally ventilated two-bay greenhouse, and a multi-bay greenhouse [13–16].

In evaluating the performance of this tool, fluid dynamic simulations have been performed by several researchers [17–19]. These numerical models allow the determination of the greenhouse microclimate interacting with plant activity, which allowed a numerical validation to be conducted with tomato crop plants. Radiative transfer models were solved within the crop, being considered a porous medium, emphasising the microclimate and plant activities (transpiration and photosynthesis).

R. W. Kim et al. [20] developed an educational virtual reality simulator for greenhouse growers. Computational fluid dynamics (CFD) simulation was performed to analyse the aerodynamic environment in the greenhouse with tomato growing. The CFD model results were validated using measured temperature and air speed in actual greenhouses. Then, several scenarios were studied to analyse the aerodynamic environment in a greenhouse with tomato crops. The CFD results were used for the link with the virtual space. This allowed the development of technology to visualise the aerodynamic environment inside greenhouses, where users can experience realistic visual effects.

Yeo et al. [21] studied the design and validation of a building energy simulator model of a plastic-covered greenhouse. The model takes into account the tomato growing pattern and natural ventilation characteristics. The model results were validated by comparing the measured temperature and humidity in the greenhouse. The results showed that the mean absolute error of the temperature was 1.57 °C and the relative humidity was 7.7%. A correlation

coefficient R^2 equal to 0.96 and 0.89 was obtained for temperature and relative humidity, respectively.

Although several studies have been performed with this thermally insulated greenhouse [6, 7].

These works have only compared the thermal performance of two greenhouses with and without solar air collectors with tomato crops. To our knowledge, we have not found any work on CFD numerical validation on a thermally insulated greenhouse with tomato crops. In this paper, we will perform a three-dimensional simulation of the heat and mass transfer in the greenhouse. Then, we will perform a numerical validation of the experimental data to the numerical data. Finally, we will precisely map the temperature, velocity and relative humidity fields.

MATERIALS AND METHODS

Description of the System and the Experimental Site

The studied greenhouse is located at the Energy Research and Technology Centre (CRTE_n) in Borj Cédria on the Mediterranean coast of North Africa, near the city of

Tunis with the following geographical coordinates: latitude $36^{\circ}43'N$ and longitude $10^{\circ}25'E$.

This greenhouse is mono-chapel type, thermally insulated on three sides, oriented from East to West and open on the Eastside. It has the following dimensions: width: 3.7 m, length: 4 m and height: 3 m in the centre. The greenhouse's south wall and roof were covered with 3 mm thick plexiglass. The northern part of the roof and the side walls (east, west and north) were covered with sandwich panels 0.6 m and 0.4 m thick, respectively (Figure 1.a). All the actual dimensions of the experimental greenhouse have been presented in Figure 1b [6]. The mono-chapel structure of the greenhouse is made of galvanised steel and fixed to the ground with concrete (Figure 1c). It is fitted with a store made up of aluminium slats which unfold on the south face at night (Figure 1d) to reduce heat loss. A tomato crop is planted in the greenhouse (Figure 1a). The greenhouse was equipped with a centrifugal fan (west side).

Experimental Setup

Type K thermocouples were used to measure temperature distributions inside the greenhouse. The horizontal air

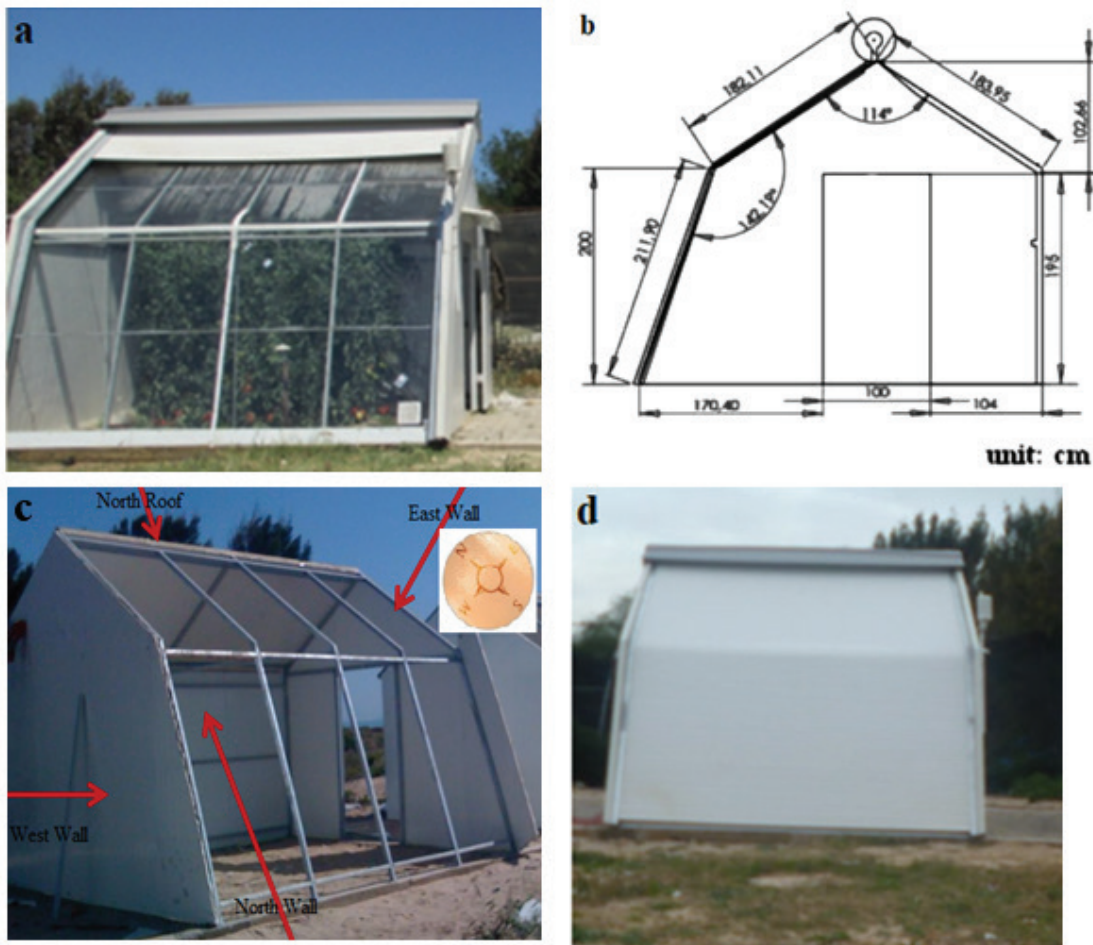


Figure 1. The experimental greenhouse [6, 7].

temperature stratification was measured at 2 m above the ground. Vertical temperature stratification was estimated at 0.10, 0.80 and 2.10 m above the ground. Measurements were taken at four levels on the greenhouse roof, outside and inside the sandwich and plexiglass panels. A sensor (HMP155A, Campbell Scientific Inc) was placed in the centre at 1.5 m above the ground to measure the relative humidity inside the greenhouse. The HMP155A sensor was housed in a 14-plate sun shield to protect it from solar irradiation. This allows air to pass freely through the protection while keeping the sensor temperature close to room temperature. Soil temperatures inside the greenhouse at different depths of 0, 0.25 and 0.5 m were measured using three PT-107 sensors. An IR120 infrared temperature sensor is used to measure the average canopy temperature. An IR-SS solar shield protects the IR120 sensor from direct solar radiation [6]. A Kipp and Zonen pyranometer measured overall solar irradiation in the horizontal plane. It is located 1.5 m above the ground in the centre of The Greenhouse. The outdoor climate parameters, that is, ambient temperature and relative humidity, are measured by an HMP155A sensor located 1.5 m above the greenhouse. Figure 2 shows the different sensors used to measure the climatic parameters inside and outside the experimental setup. These measured climate parameters are samples recorded every 10 minutes using a CR5000 data logger (Campbell Scientific Inc).

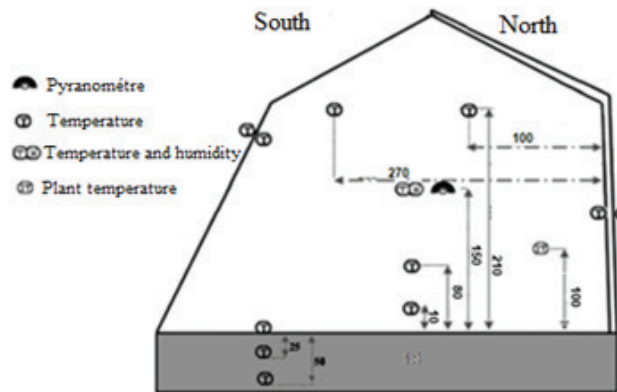


Figure 2. The various measuring sensors in the greenhouse [6].

Physical Characteristics of the Greenhouse

The physical properties of the greenhouse elements, that is, the Plexiglas cover, the crop cover and the soil, are listed in Table 1. The canopy and Plexiglas cover reflectivity and transmissivity spectra are recorded in the wavelength range (380-900 nm). Reflectivity and transmissivity spectra are recorded using the LAMBDA950 UV-vis-NIR spectrometer equipped with an integrating sphere.

Table 1. Cover, canopy, and soil characteristics [7].

Materials	Cover	Canopy	Soil
Reflectivity for solar radiations	0.10	0.1	0.2
Transmissivity for solar radiations	0.85	0	0
Emissivity	0.02	0.05	0.84
Reflectivity for thermal radiations	0.10	0.55	0.16
Transmissivity for thermal radiations	0.88	0.4	0

Greenhouse Culture

A local variety of tomatoes, “Colibri”, was planted on the ground inside the greenhouse. The plants are arranged in 4 rows with 7 tomato plants in each row, and the rows are spaced 40 cm apart. A drip system irrigates the plants.

THEORY

The modelling of heat and mass transfer flows in a given configuration consists of determining the characteristic variables of the fluid under consideration (temperature, speed, pressure, relative humidity, etc.) at any point in the study area and at any time. In the case of our study, the fluid used is a mixture of air and water vapour, whose physical properties are given in Table 2.

Position of the Problem

A 3D model was used in this work to study the greenhouse with tomato plants. We represent, in figure 3, the geometry of the simplified 3D model with rows of tomatoes. This configuration considers only the greenhouse domain and its internal environment to minimise the computation time. The greenhouse door was left open during the day

Table 2. Physical properties of components

Materials	Thickness (mm)	ρ (kg m ⁻³)	Cp (J K ⁻¹ kg ⁻¹)	λ (W m ⁻¹ K ⁻¹)	Refractive index (-)	Emissivity
Plexiglas	3	1180	1470	0.19	1.49	0.9
Polyurethane sandwich insulation panels	40	40	1000	0.028	1.486	0.6
Soil	-	1620	1480	2.5		0.84
Air	-	1.22	1006	0.0242	1	
Water vapour[15]	-	0.554	f(T)	0.0261	1	

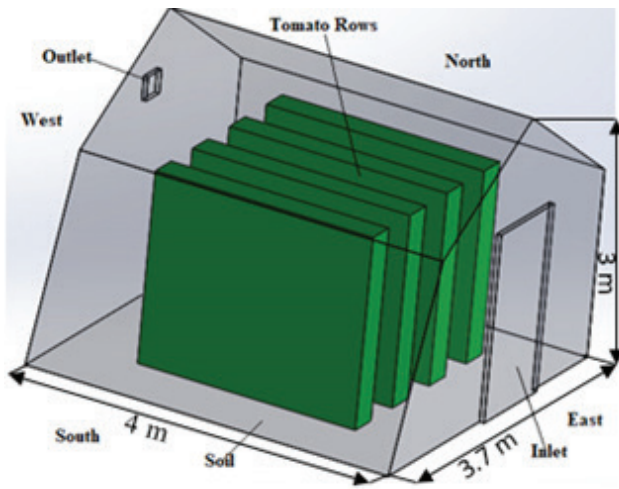


Figure 3. Geometry of the simplified model of the greenhouse with cultivation.

to avoid very high temperatures. To simplify calculations, crops in the greenhouse were modelled as porous blocks, as in several works [17, 18, 19]. They are organised in 4 parallelipedal rows with an average height of 190 cm and a volume of 2,508 m³. The distance between two consecutive blocks is 40 cm (Figure 3).

Fundamental Equations

We have established the following assumptions to write the differential equations involved in this study of greenhouse microclimate:

- The medium is continuous, isotropic
- The heat storage capacity of sandwich panels (walls and roof) is neglected.
- Multiple heat exchange by radiation between roofs and walls is neglected.
- Heat exchange between the air and the sandwich panels (roof and walls) is neglected.

To model the physical variation Φ equations representing the amount of transport, specifically mass (mass fraction of air and water vapour), the amount of motion and energy for a three-dimensional flow. The transport equation is written in the following general form [17]:

$$\frac{\partial \Phi}{\partial t} + \frac{\partial(\rho \Phi U_i)}{\partial x_j} = \frac{\partial}{\partial x_j} \left(\Gamma_\Phi \frac{\partial \Phi}{\partial X_j} \right) + S_\Phi \quad (1)$$

Or U_i (m.s⁻¹) represents the three variables (u, v and w) of the velocity vector, Γ_Φ is the diffusion coefficient and S_Φ is the source term of Φ . The transports equations for each physical quantity Φ and each source term S_Φ describing the interactions between climate parameters and plants are detailed in the work of [18, 19].

The transport equations modelling the physical phenomena described above are as follows:

Continuity equation

It is obtained by conserving the mass between the mass flows entering an element and those leaving, which is expressed as follows [22]:

$$\frac{\partial \rho}{\partial t} + \nabla \cdot (\rho \vec{v}) = 0 \quad (2)$$

Or: ρ is the density and $\vec{v}(u, v, w)$ is the components of the velocity vector.

The density can be considered constant except in the buoyancy force term, so the conservation of mass equation takes the same form as that for an incompressible fluid.

Momentum conservation equation

The rate of change of the amount of motion contained in the control volume is equal to the sum of all external forces applied to it:

$$\rho \frac{\partial u_i}{\partial t} + \rho \left(u_j \frac{\partial u_i}{\partial x_j} \right) = - \frac{\partial P}{\partial x_i} + \mu \left(\frac{\partial^2 u_i}{\partial x_j^2} \right) - \rho g \delta_{i3} + \rho F_i \quad (3)$$

With $\rho g \delta_{i3}$, is the force of gravity and ρF_i , is the buoyancy force.

Energy conservation equation

The energy change of a fluid particle is equal to the heat input and the work done on the particle.

$$\rho C_p \frac{\partial T}{\partial t} + u_j \rho C_p \frac{\partial T}{\partial x_j} = \frac{\partial}{\partial x_j} \left[\lambda \frac{\partial T}{\partial x_j} \right] + \Phi + S_m \quad (4)$$

Since the viscous dissipation term Φ is negligible compared to the diffusion heat transfers, the energy equation becomes:

$$\frac{\partial T}{\partial t} + u_j \frac{\partial T}{\partial x_j} = \frac{\partial}{\partial x_j} \left[a \cdot \frac{\partial T}{\partial x_j} \right] + \frac{S_m}{\rho C_p} \quad (5)$$

With $a = \frac{\lambda}{\rho C_p}$, the thermal diffusivity of the fluid in m² s⁻¹.

Species conservation equation (mass transfer)

In this study, the fluid is considered as a mixture of two species: air and water vapour. The mass fraction y_m of each component m in the fluid can be determined by solving the diffusive-convective transport equation of the air mass fraction and the water mass fraction [22]:

$$\frac{\partial(\rho y_m)}{\partial t} + \frac{\partial}{\partial x_j} (\rho y_m u_i) = - \frac{\partial}{\partial x_j} \cdot J_m + s_m \quad (6)$$

With y_m is the mass fraction of a species m defined by:

$$y_m = \frac{m_m}{\sum m_i} \quad (7)$$

With m_m (kg) the mass of species m . Our mixture is binary; we can write: $y_{air} + y_{vapour} = 1$.

The term J_m is expressed with Fick's law:

$$J_m = -\rho D_{m,a} \frac{\partial y_m}{\partial x_j} \quad (8)$$

With $D_{m,a}$ is the diffusion coefficient of species m in air.

In the case of water vapour, the diffusion coefficient $D_{m,a}$ is estimated by the Schmeer relation:

$$D_{m,a} = 2.26 \cdot 10^{-5} \frac{1}{p} \left(\frac{T}{273} \right)^{1.81} \quad (9)$$

Where p pressure in bar, T temperature in K and $D_{m,a}$ in $m^2 s^{-1}$.

We adopt the standard $k-\varepsilon$ model in this study. This model has been widely used in the literature and has been found to be reliable for air change prediction [20, 24].

The Boussinesq model has been taken into account, which means that the buoyancy force due to the difference in air density is added as a source term in the momentum equation. The Boussinesq approximation allows the density variables to be neglected in the conservation equations, except for its implication as a driving force in the momentum conservation equation.

$$\rho = \rho_0 (1 - \beta(T - T_0)) \quad (10)$$

The driving force F_i of free or mixed convection can be expressed as:

$$F_i = (\rho_0 - \rho)g_i = \beta\rho_0(T - T_0)g_i \quad (11)$$

With β the coefficient of expansion; T_0 , ρ_0 , reference temperature and density at the operating conditions, respectively.

These buoyancy forces were taken into account using the perfect gas model. This characterizes the coupling between the energy equation and the vertical component of momentum equation which was modelled using the temperature dependence of the air density and the water vapor mixture [18, 19, 25].

In a fluid made up of several species, the law of perfect gases is used. This law allows to take into account the variation of density not only as a function of temperature as in the case of the Boussinesq approximation, but also of the concentration of species present in a volume of fluid. The density in this case is defined as a function of temperature and the mass fraction of the species. It is expressed in the form of the law of perfect gases [25]:

$$\rho = \frac{P_{op}}{RT \sum_i \frac{y_i}{M_i}} \quad (12)$$

With $R = 8,31 \text{ J Mol}^{-1} \text{ K}^{-1}$ is the universal gas constant, P_{op} (Pa) is the operating pressure, y_i (kg kg^{-1}) is the mass fraction of the species i et M_i (kg mol^{-1}) is the molecular weight of the species i .

Radiative Transfer Model

The discrete ordinate (DO) model was used to solve the radiative transfer equation (RTE) for a finite number of discrete solid angles. Each solid angle is associated with a fixed vector direction in the global Cartesian system, and this is instead of adding additional heat sources [26]. This model allows the coupling of convective transfers and radiation exchanges at the level of the optical properties of the considered media. The DO model is most commonly used for greenhouse microclimate studies [19, 25, 27], as it can cover the full range of wavelengths in the spectrum [28] (see Table 1). The equation used in the DO model allows Fluent to model non-grey radiation using a grey band model. This model is described in the Fluent Inc. 19.2 user guide [29] and also in several books [26, 30]:

$$\begin{aligned} \nabla \cdot (I_\lambda(\vec{r}, \vec{s}) \vec{s}) + (a_\lambda + \sigma_s) I_\lambda(\vec{r}, \vec{s}) = \\ a_\lambda I_{b\lambda} + \frac{\sigma_s}{4\pi} \int_0^{4\pi} I_\lambda(\vec{r}, \vec{s}') \Phi(\vec{s}, \vec{s}') d\Omega' \end{aligned} \quad (13)$$

Since λ is the wavelength, a_λ is the spectral absorption coefficient, \vec{s} is the direction vector, \vec{s}' is the scattering direction vector, σ_s is the scattering coefficient and $I_{b\lambda}$ is the blackbody intensity given by Planck's function. The DO model makes it possible to define the physical optical properties of transparent, semi-transparent and opaque media to consider the net contribution of radiation per unit volume in the energy equation [19].

Modelling within the Culture

As in several works, the cultures were considered as porous media with a solid matrix having pores [17, 18, 19, 25]. This phenomenon is modelled by the Darcy-Forchheimer equation (Eq. 14). Table 3 shows the equivalent thermal properties of the tomato crop in water and dry matter [19].

The crops thus create resistance to air movement in the greenhouse [14]. The drag coefficient value $C_D = 0.32$

Table 3. Equivalent thermal properties of the tomato crop in water and dry matter [19].

	Water	Dry matter
At 25°C		
ρ (kg m^{-3})	997.05	700
C_p ($\text{J kg}^{-1} \text{K}^{-1}$)	4181.66	2310
λ ($\text{W m}^{-1} \text{K}^{-1}$)	0.6069	0.173
μ ($\text{kg m}^{-1} \text{s}^{-1}$)	8.92e-4	-

has been used in many CFD models for a tomato crop in a greenhouse [17, 31]. In Fluent, the Forchheimer equation is given in the following form [29]:

$$\vec{\nabla} p = -C_0 \|\vec{V}\|^{C_1-1} \cdot \vec{V} \quad (14)$$

For tomato vegetation, the coefficients $C_0 = 1.32$ et $C_1 = 2$.

In order to take into account the radiation within the crop, the crop is considered as non-diffuse [25], which leads us to consider only the direct fraction of solar radiation in this sub-model of the crop. However, as suggested by some work [19], the canopy has been considered as a semi-transparent medium with optical properties (Table 1), and this is in order to solve the radiative equations using the DO model. The Beer-Lambert law also allows the determination of the fraction of the solar radiation flux absorbed by the vegetation, which is given as follows [7, 19].

$$\alpha_v = (1 - \rho_v) e^{-k_v LAI} \quad (15)$$

$$\tau_v = (1 - \rho_v - \alpha_v) \quad (16)$$

$k_v = 0.75$ [19] is the canopy attenuation coefficient, LAI is the leaf area index and α_v , τ_v et ρ_v are the solar absorption, transmission and reflection coefficients of the vegetation. This flux of solar radiation absorbed by the canopy also produces water vapour and sensible heat [7].

Model Performance Evaluation

The model performance was evaluated in quantitative terms using relative root mean square error (rRMSE), the per cent error [11]:

$$rRMSE = \frac{100}{\bar{y}} \left(\sqrt{\frac{\sum (y_m - y_{es})^2}{n}} \right) \quad (17)$$

$$Per\ cent\ error = \frac{(y_m - y_{es})}{y_m} \times 100 \quad (18)$$

Where y_m is the measured data; y_{es} is the estimated data; n is the number of data points; and \bar{y} is the mean value of measured data.

Boundary Conditions

The boundary conditions are of imposed wall types to limit the study area to the dimensions of the greenhouse. The outdoor climate conditions were used as input parameters for the simulation. In Figure 4, we show the daily variations of the ambient outdoor air temperature, solar irradiation and relative air humidity. These values are the sets of measurements made during the day of the experiment for steps of 10 minutes.

The ambient temperature of the outside air varies from 292.9 °K to 296.7 °K between 9:40 and 11h30 and remains almost constant until 13:20 with a value of 296.82 °K and then decreases to 287.2 °K at 18:00. The global solar irradiance varied from 264 W/m² to 557 W/m² between 9:40 and 13:10 and decreased considerably until 18:00.

We observe a variation of the relative humidity of the ambient air as a function of time. The relative humidity of the ambient air increases due to the low value of solar irradiation. At the beginning of the day, the humidity was 73.5%, which increased to 74.67% at 11:10 and decreased to 72.96% at 18:00. The average value of the outdoor relative humidity was 73.9%.

The adiabatic condition was imposed on the insulated walls. The boundary conditions of the studied greenhouse area are shown in Table 4.

NUMERICAL MODEL

Numerical Methods

The Ansys-Fluent CFD code (version 19.2) is used to explicitly calculate the temperature and relative humidity distribution of the air in the greenhouse. This code uses the finite volume method to solve the Navier-Stokes conservation equations numerically. The 3D simulation is adopted to better take into account the whole structure and elements of the greenhouse. A set of quasi-steady-state simulations was performed for fixed boundary conditions. A

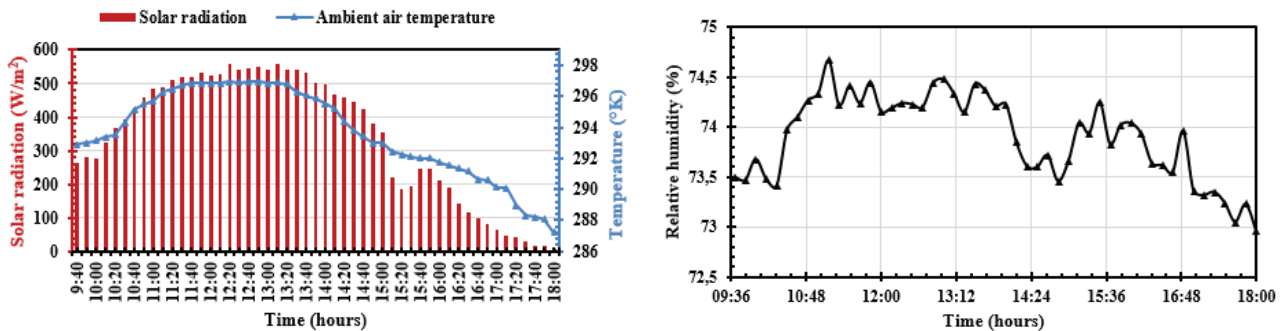
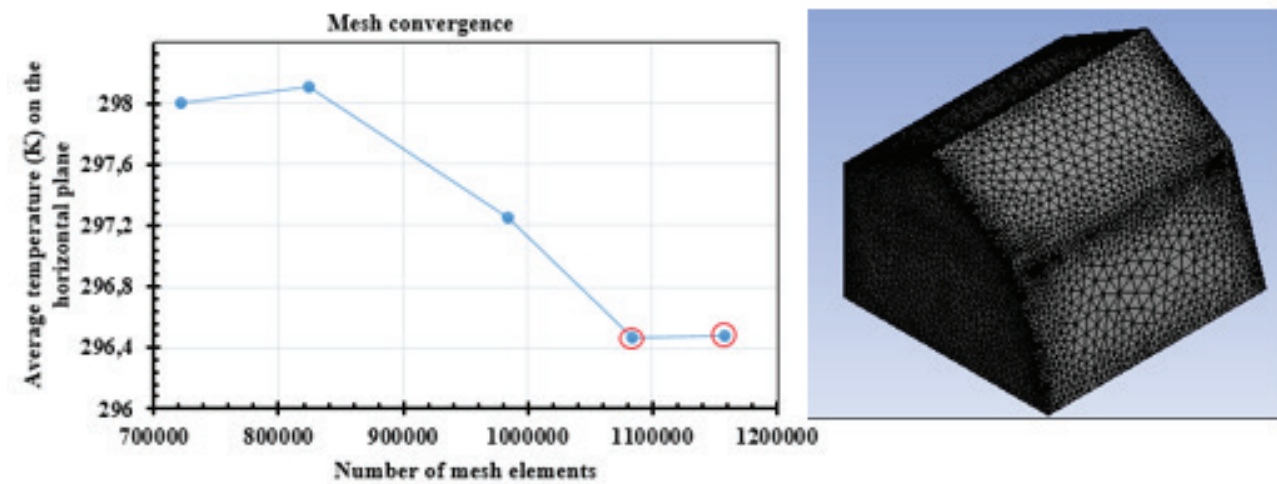


Figure 4. Daily variations of ambient outdoor air temperature, solar irradiation and relative air humidity.

Table 4. Greenhouse boundary conditions as of April 30.

Parameters	Momentum equation	Energy equation	Radiation equation	Species equation (water vapour)
Sandwich panel walls and roof	Stationary wall No-slip condition	Adiabatic conditions	Opaque and diffuse wall Internal émissivity = 0.6	
Plexiglass wall and roof	Stationary wall No-slip condition	Imposed flux (values measured during the experiment)	Semi-transparent Radiation flux passing through the imposed wall (values measured every 10 minutes)	
Door (open)	Outflow			
Window	Exhaust-fan Intensity and viscosity ratio Turbulent intensity 5%	Imposée average discharge temperature (298.15K)		Backflow specifies mass fraction H_2O (calculated for each measurement)
Culture	Stationary wall No-slip condition	Coupling condition between the walls and the floor of the greenhouse	Semi-transparent and non-diffusive	Specified mass fraction H_2O (calculated for each measurement)
Greenhouse soil (homogeneous all surfaces)	Stationary wall No-slip condition	Imposed temperature (value measured during the experiment)	Opaque and diffuse wall Internal emissivity = 0.84	Specified mass fraction H_2O (calculated for each measure)

**Figure 5.** Sensitivity study of the mesh on the results.

second-order pressure-based discretisation scheme with velocity-pressure coupling is used in order to obtain good accuracy and without the risk of divergence in the calculations. The SIMPLEC method has been used for the coupled pressure and velocity pulse to improve the convergence of the iteration process. The convergence criterion for all variables was 10^{-6} and the relaxation factors are 0.3 for water vapour, kinetic energy, dissipation rate, turbulent viscosity and 0.5 for DO, energy, pressure, density, body forces and momentum.

Adopted Mesh

Particular attention was paid to the meshes to test their stability and sensitivity to simulation results. Five mesh densities were tested with an element size of 0.31395 m. The average temperature in the horizontal plane at 2 m from the ground was recorded for each cell. The mesh is considered stable when the difference between two temperature values for two consecutive meshes (1084231 and 1158614 elements) is 0.013 K. Thus, the grid of 1084231 elements was kept for the rest of the simulation with finer resolutions

imposed near the ground, roof, walls and crops. In figure 5, we present a mesh sensitivity study on the results.

RESULTS AND DISCUSSION

Model Validation

The greenhouse model was simulated based on the assumption of a sunny day. There were 9 instantaneous data points for the day, accumulated from 10h00 to 18h00. The validation of the model is mainly based on the comparison of the results of the numerical values and the experimental values. This comparison especially concerns the average air temperature, the air temperature at different points, the plant temperature at one end and the relative air humidity inside the greenhouse.

Temperature comparison

Figure 6 shows the air temperature variation curves as a function of time. Figure 6A represents the average air temperature in the greenhouse, and Figure 6B, C and D are the temperature curves at different points. The model's performance was evaluated using the coefficient of determination R^2 , percentage error, and relative error.

Figure 6A presents the variation curve of the average air temperature in the greenhouse. It can be seen that the model underestimates the observations. In the beginning, between 10:00 and 14:00, the temperature difference is less important, with values of 2.71 °C and 1.45 °C, respectively.

However, from 14:00 to 18:00, the temperature difference becomes more important, with a value of 4.49 °C. These deviations are related to the difference in temperature that was observed between the predicted temperatures at different points, which may be related to the phenomenon of plant evapotranspiration which was not taken into account in the simulation. Using a regression curve, we determined a correlation coefficient $R^2 = 0.89$ was found between the simulated and measured values, with an average percentage error of 0.88%.

Figures 6B, C and D presents the air temperature variations at different points in the greenhouse. Figure 6B shows the variation in air temperature at 10 cm above the ground. The simulated air temperature values underestimate the observations. It is observed that the variation of the simulated air temperature follows the trend of the curve of the measured values. The difference between the air temperatures is slight at first and becomes more significant between 12:00 and 18:00; for respective values of 1.08 °C and 1.59 °C. The coefficient of determination $R^2 = 0.774$ with a percentage error < 5%.

Figure 6C presents the variation of the air temperature at 80 cm above the ground. It is observed that the variation of the simulated air temperature follows the variation of the measured air temperature. At the beginning, the simulated values overestimate those of the observations between 10:00 a.m. and 2:00 p.m. with a small temperature difference. It becomes more important between 3:00 p.m. and 6:00 p.m. and underestimates the observed values.

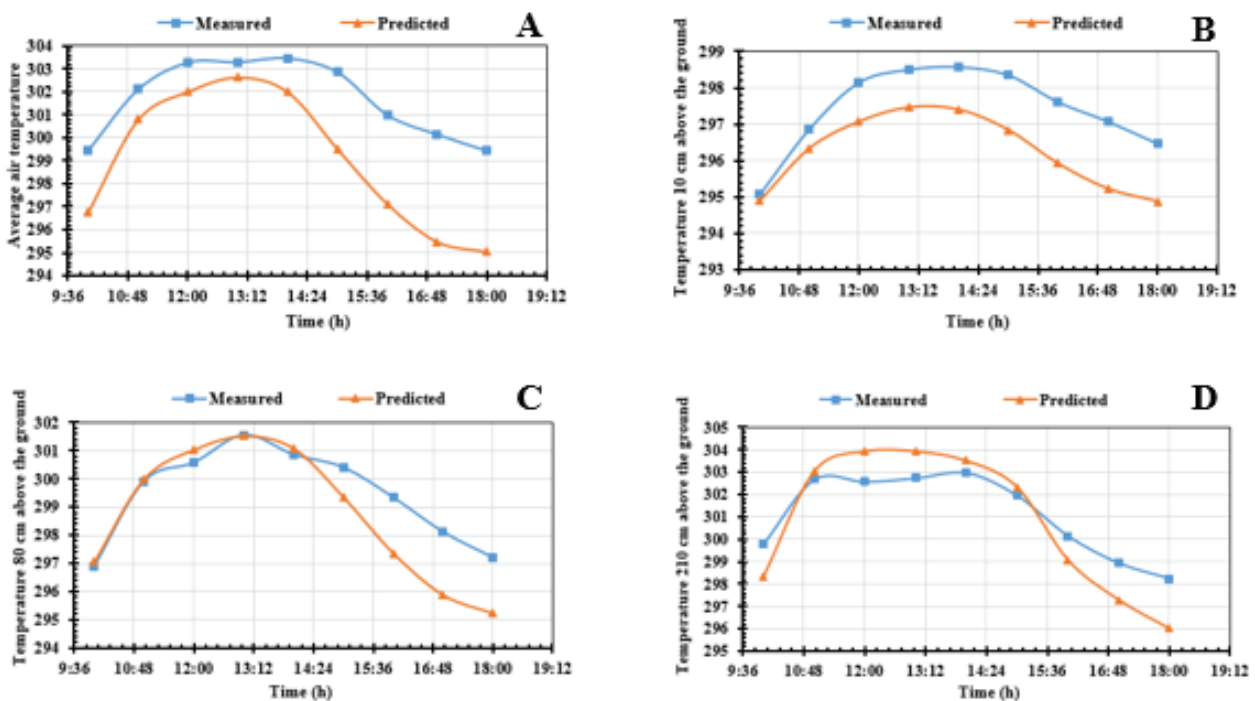


Figure 6. Comparisons of air and plant temperature in the greenhouse.

The maximum difference is obtained from 5:00 p.m. for a value of 2.22°C and a correlation coefficient $R^2=0.836$ was obtained between the measured values and those observed with a percentage error < 5%.

Figure 6D shows the variation in air temperature at 210 cm above the ground. The variation in simulated air temperature underestimates at the start and between 4 p.m. and 6 p.m., but begins to overestimate between 11 a.m. and 3 p.m. The highest temperature difference was obtained at 6 p.m. for a value of 2.23°C. A correlation coefficient $R^2=0.987$ is obtained with a low percentage error < 5%.

These predictions agree well with the observed values, with a relatively low percentage error < 5% with a correlation coefficient between 0.774 and 0.987. It can be said that the model predicts the air temperature inside the greenhouse quite well.

Figure 7 shows the temporal evolution of the measured and simulated plant temperature.

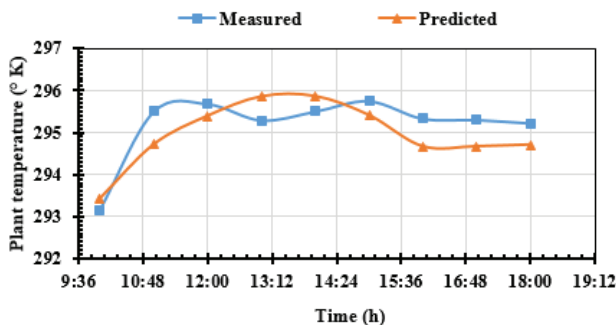


Figure 7. Measured and simulated plant temperature variations in the greenhouse.

The model first underestimates the measured values between 10:00 and 12:00, then overestimates them until 15:00 and underestimates them until 18:00. The most significant temperature difference is 0.785 °C, found at 16:00. The model result is satisfactory, with an observed relative error of 0.16 and a coefficient of determination $R^2=0.628$. This low value of R^2 between the simulated and experimental values is due to the absence of the plant evapotranspiration phenomenon and also to the watering of the plants which was not taken into account.

These observed deviations between the measured and predicted values may be due to the dynamic air conditions that were not considered in the simulation. Therefore, the heat losses in the greenhouse are mainly related to the door's opening by the natural ventilation effect.

Variation in relative humidity inside the greenhouse

The greenhouse air's relative humidity was studied in the centre at 1.5 m above the ground. Figure 8 represents the curves of the variation of the relative humidity of the air in the greenhouse.

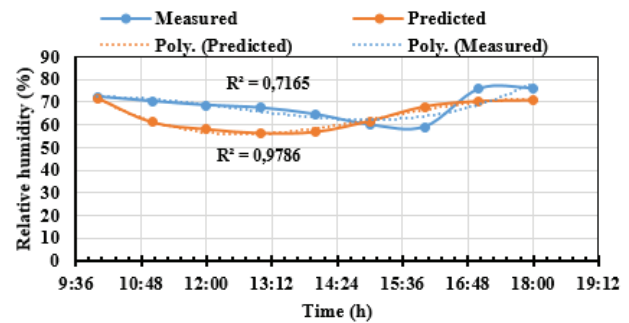


Figure 8. Variation of relative air humidity with time (measured and simulated) in the greenhouse.

We see that the model starts by overestimating relative humidity values on the time series of measurements. It underestimates these values and ends the series by overestimating the measured values. This is mainly due to the variation in the speed of the air renewal in the greenhouse through the door. This renewable air flow rate is a function of the outside wind speed, which allows moisture to be exhausted to the outside. These experimental parameters have not been considered in our simulation model and the plants' physiological phenomena (evapotranspiration). All these factors can explain the differences between the measured and simulated relative humidity values inside the greenhouse. The model describes a normal behaviour of relative humidity's evolution as a time function. The fourth-order polynomial curve obtained the results of the coefficient of determination, $R^2 = 0.9786$ for the simulated relative humidity and $R^2 = 0.7165$ for the measured relative humidity values. Table 5 shows the comparison of the validation results based on the performance of the numerical model.

Mapped the Indoor Climate of the Greenhouse

The numerical model validation was based mainly on the temporal variation of temperature and humidity in the greenhouse. The CFD model will provide more detailed images of the climate, mapping the greenhouse spaces in two dimensions. We also present the air velocity fields in the greenhouse. Figure 9 shows the temperature, velocity and relative humidity fields on a vertical plane in the centre of the greenhouse.

It is observed that the temperature is higher towards the southern part of the greenhouse at 13:00 (Figure 9A). This is mainly related to the transparent nature of the Plexiglas on the south wall, unlike the other thermally insulated walls, which are opaque to solar radiation. This temperature distribution remains heterogeneous as it propagates towards the greenhouse's interior. It is more noticeable on the crop rows next to the south wall.

Figure 9B shows the distribution of the air relative humidity in the greenhouse. It can be seen that the relative

Table 5. Comparison in terms of numerical model performance

Case study	Parameter of comparison
Md.S. Ahamed et al [11].	The comparison between simulated and measured values of soil temperature has for values $R^2 = 0.68$, $RMSE = 1.8\text{ }^\circ\text{C}$ and $rRMSE = 9.35\%$. At the north wall, $R^2 = 0.77$, $RMSE = 2.2\text{ }^\circ\text{C}$ and $rRMSE = 11.9\%$ were found.
P.E. Bournet et al [25].	The well-watered plants, $R^2 > 0.91$ and $RMSE < 1.56\text{ K}$ for all temperatures and plants under restricted water conditions, with R^2 higher than 0.86 and $RMSE$ lower than 1.87 K. The results obtained for relative humidity: $R^2 > 0.94$ and $RMSE < 10\%$ for well-watered plants, and $R^2 > 0.78$ and $RMSE < 6.69\%$ for the restricted water case.
Edwin A. Villagran et al [32].	The coefficient of determinations (R^2) found ranged from 0.893 to 0.968 for temperature versus time. An R^2 value between 0.752 and 0.815 was obtained for air speed.
Our case	The coefficient of determinations (R^2) found ranged from 0.628 to 0.987 for temperature versus time with an $rRMSE < 5\%$. The most significant temperature difference was obtained in the average air temperature inside the greenhouse which has a value of 4.69 $^\circ\text{K}$.

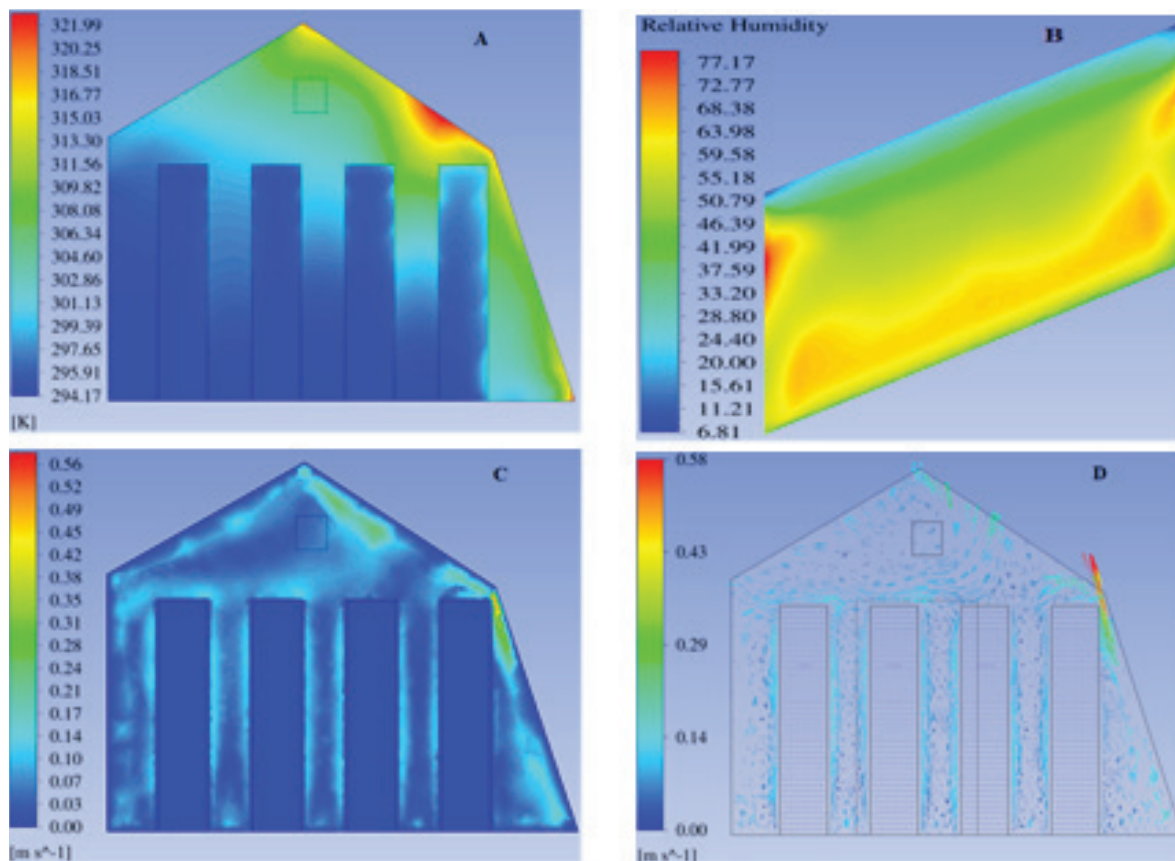


Figure 9. Distribution of air temperature (A), relative humidity (B), air velocity (C) and velocity vector (D) in the centre of the greenhouse at 13:00.

humidity is higher at the crops, the door and the window. This shows that the air humidified by the crops is either evacuated through the door or the window to the outside. The relative humidity of the air is higher at the crop level, which is mainly due to the evapotranspiration phenomenon of the plants. Moreover, the water from the plants' watering evaporates at the ground level. We also note for the renewal,

the door constitutes the entrance of new humid air, and the window is the exit of humidified air, that is why we observe traces of humidity in these levels.

Figure 9C shows the air velocity distribution in the greenhouse. It can be seen that the air velocity is low, with a maximum of 0.56 m/s. This low velocity shows that the crop rows provide resistance to air movement. We note a

fairly clear distribution of air velocity between the rows, as no resistance is encountered Higher air velocities were obtained at the fen. We can see in figure 9D the velocity vectors created by the turbulence of the air in the greenhouse. These turbulent velocity vectors are recorded on the window part of the greenhouse. This shows the effect of air extraction through the window.

Figure 10 shows the horizontal distribution of temperature (A, A1), humidity (B, B1) and speed (C, C1) at different heights

Figure 10 A and A1 show the air temperature distribution at different positions in the greenhouse. It is observed that the air temperature is low at the level of the crop rows for a maximum value of 314.59 °K compared to the top of

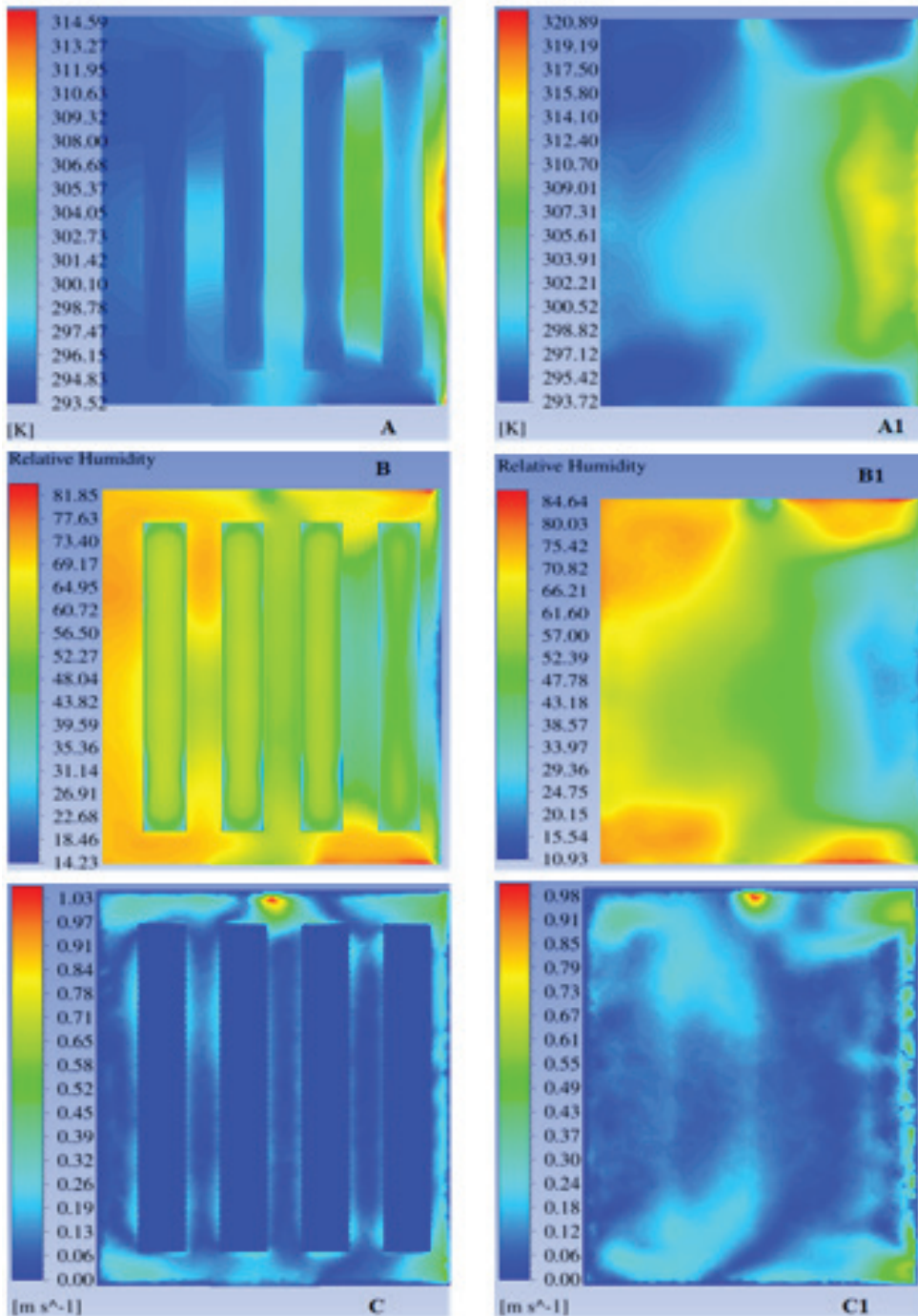


Figure 10. Horizontal temperature, relative humidity and air velocity distribution at 1.5 m above ground (A, B, C) and 2 m above ground (A1, B1, C1) in the greenhouse at 13:00.

the canopy for a maximum value of 320.89 °K or a difference of 6.3 °K. This is due to the cooling of the air at the crop level. There is also an increase in air temperature from the north wall to the south wall. This shows the ability of the south wall to let the sun's rays through its transparent wall. The air temperature is higher at 2 m than at 1.5 m because of the rising warm air.

Figure 10 B and B1 show the distribution of the relative humidity of the air at different positions in the greenhouse. The humidity is more distributed at the crop rows than above the canopy. This shows the difficulty of the humidified air to escape upwards. The humidity is also higher on the side of the insulated walls, which is also an area of low air temperature.

Figure 10 C and C1 show the air velocity distribution at different positions in the greenhouse. The airspeed is not homogeneous everywhere in the greenhouse. It can be seen that the velocity is higher above the canopy at 2 m than at 1.5 m from the ground at the rows. The average value is 0.54 m/s and 0.51 m/s, respectively, at 2 m and 1.5 m above the ground. This shows the resistance to air movement by the crop rows in the greenhouse.

CONCLUSION

A solar greenhouse was modelled with a tomato crop inside. The model considered the crop a porous medium consisting of dry matter and water vapour to couple the greenhouse heat and mass transfer exchanges. The discrete ordinate (DO) model was used to solve the radiative transfer equation. The CFD numerical model's results were compared with the experimental values. The results of the study are expressed as follows:

A good agreement was found between the measured and simulated temperature values at different positions in the greenhouse, with error percentages of less than 5%. The polynomial curve of order 4 gave the results of the coefficient of determination of $R^2 = 0.9786$ for the simulated relative humidity values and of $R^2 = 0.7165$ for the measured relative humidity values.

The simulation results show that the air velocity distribution is not homogeneous, it is more important above the canopy than below, but an average of 0.525 m/s is found between 1.5 m and 2 m on a horizontal plane.

NOMENCLATURE

a	Thermal diffusivity
a_λ	Spectral absorption coefficient
C_0, C_1	Power law constant
C_D	Drag coefficient of the vegetation (-)
C_p	Specific heat of the air (J kg ⁻¹ K ⁻¹)
$D_{m,a}$	Diffusivity coefficient of species m in air (m ² s ⁻¹)
F	External forces
g	Gravitational acceleration (m s ⁻¹)

I_λ	Monochromatic radiation intensity (W m ⁻³)
J_m	Diffusion flux of species m
k	Turbulent kinetic energy (m ² s ⁻²)
k_v	Vegetation attenuation coefficient
LAI	Leaf area index
M_i	The molecular mass of species i (kg mol ⁻¹)
P	Pressure (Pa)
Pop	The operating pressure (Pa)
R	Universal gas constant (J mol ⁻¹ K ⁻¹)
RH	Relative humidity (%)
\vec{r}	Position vector
\vec{s}	Direction vector
\vec{s}'	Scattering direction vector
S_m	Source thermal of the conservation of mass equation
S_Φ	Source term for Φ
t	Time (s)
T	Temperature (K)
U_i	Three components of velocity (m s ⁻¹)
γ_m	Mass fraction
γ_i	Mass fraction of species i (kg kg ⁻¹)

Greek symbols

β	Extinction or attenuation coefficient, m ⁻¹
λ	Thermal conductivity (W m ⁻¹ K ⁻¹)
μ	Viscosity of air (kg m ⁻¹ s ⁻¹)
ρ	Turbulent kinetic energy (m ² s ⁻³)
ε	Turbulent kinetic energy (m ² s ⁻³)
Ω	Solid angle (-)
Φ	Physical quantity
Γ_Φ	Diffusion coefficient
σ_s	Scattering coefficient

AUTHORSHIP CONTRIBUTIONS

Authors equally contributed to this work.

DATA AVAILABILITY STATEMENT

The authors confirm that the data that supports the findings of this study are available within the article. Raw data that support the finding of this study are available from the corresponding author, upon reasonable request.

CONFLICT OF INTEREST

The author declared no potential conflicts of interest with respect to the research, authorship, and/or publication of this article.

ETHICS

There are no ethical issues with the publication of this manuscript.

REFERENCES

- [1] Ferreira AG, Maia CB, Cortez AFB, Valle RM. Technical Feasibility Assessment of Solar Chimney for Food Drying. *Renew Energy* 2009;34:217–222.
- [2] United Nations, Department of Economic and Social Affairs. *World Population Prospects 2017*. [Internet]. New York. Available at: <https://www.un.org/development/desa/fr/news/population/world-population-prospects-2017> Last Accessed Date: 21.07.2017.
- [3] Food and Agriculture Organization. *La faim ne diminue toujours pas dans le monde depuis trois ans et l'obésité est toujours à la hausse - Rapport des Nations Unies*. New York. Available from: <http://www.fao.org/news/story/fr/item/1201888/icode/> Last Accessed Date: 15.07.2019.
- [4] Mistriotis A, Arcidiacono C, Picuno P, Bot GPA, Scarascia-Mugnozza G. Computational analysis of ventilation in greenhouses at zero- and low-wind-speeds. *Agric For Meteorol* 1997;88:121–135. [\[CrossRef\]](#)
- [5] Boulard T, Haxaire R, Lamrani MA, Roy JC, Jaffrin A. Characterization and Modelling of the Air Fluxes induced by Natural Ventilation in a Greenhouse. *J Agric Eng Res* 1999;74:135–144. [\[CrossRef\]](#)
- [6] Bouadila S, Kooli S, Skouri S, Lazaar M, Farhat A. Improvement of the greenhouse climate using a solar air heater with latent storage energy. *Energy* 2014;64:663–672. [\[CrossRef\]](#)
- [7] Kooli S, Bouadila S, Lazaar M, Farhat A. The effect of nocturnal shutter on insulated greenhouse using a solar air heater with latent storage energy. *Sol Energy* 2015;115:217–228. [\[CrossRef\]](#)
- [8] Naseer M, Persson T, Righini I, Stanghellini C, Maessen H, Verheul MJ. Bio-economic Evaluation of Greenhouse Designs for Seasonal Tomato Production in Norway. *Biosystems Eng* 2021;212:413–430. [\[CrossRef\]](#)
- [9] Jain D, Tiwari GN. Effect of greenhouse on crop drying under natural and forced convection I: Evaluation of convective mass transfer coefficient. *Energy Convers Manag* 2004;45:765–783. [\[CrossRef\]](#)
- [10] Kumar A, Tiwari GN. Thermal modeling of a natural convection greenhouse drying system for jaggery: An experimental validation. *Sol Energy* 2006;80:1135–1144. [\[CrossRef\]](#)
- [11] Ahamed MS, Guo H, Tanino K. Development of a thermal model for simulation of supplemental heating requirements in Chinese-style solar greenhouses. *Comput Electron Agric* 2018;150:235–244. [\[CrossRef\]](#)
- [12] Tonga G, Christopher DM, Li B. Numerical Modelling of Temperature Variations in a Chinese Solar Greenhouse. *Comput Electron Agric* 2009;68:129–139. [\[CrossRef\]](#)
- [13] Boulard T, Wang S. Experimental and numerical studies on the heterogeneity of crop transpiration in a plastic tunnel. *Comput Electron Agric* 2002;34:173–190. [\[CrossRef\]](#)
- [14] Bartzanas T, Boulard T, Kittas C. Effect of vent arrangement on windward ventilation of a tunnel greenhouse. *Biosyst Eng* 2004;88:479–490. [\[CrossRef\]](#)
- [15] Bournet PE, Boulard T. Effect of Ventilator Configuration on the distributed climate of greenhouses: A review of experimental and CFD Studies. *Comput Electron Agric* 2010;74:195–217. [\[CrossRef\]](#)
- [16] Benni S, Tassinari P, Bonora F, Barbaresi A, Torreggiani D. Efficacy of greenhouse natural Ventilation: Environmental monitoring and CFD simulations of a study case. *Energy Build* 2016;125:276–286. [\[CrossRef\]](#)
- [17] Majdoubi H, Boulard T, Fatnassi H, Bouirden L. Airflow and microclimate patterns in a one-hectare canary type greenhouse: An experimental and CFD assisted study. *Agric For Meteorol* 2009;149:1050–1062. [\[CrossRef\]](#)
- [18] Nebbali R, Roy JC, Boulard T. Dynamic simulation of the distributed radiative and convective climate within a cropped greenhouse. *Renew Energy* 2012;43:111–129. [\[CrossRef\]](#)
- [19] Boulard T, Roy JC, Pouillard JB, Fatnassi H, Grisey A. Modelling of micrometeorology, canopy transpiration and photosynthesis in a closed greenhouse using computational fluid dynamics. *Biosyst Eng* 2017;158:110–133. [\[CrossRef\]](#)
- [20] Kim RW, Kim JG, Lee IB, Yeo UH, Lee SY, Decano-Valentin C. Development of three-dimensional visualisation technology of the aerodynamic environment in a Greenhouse using CFD and VR technology, part 1: Development of VR a database using CFD. *Biosyst Eng* 2021;207:33–58. [\[CrossRef\]](#)
- [21] Yeo UH, Lee SY, Park SJ, Kim JG, Choi YB, Kim RW, et al. Rooftop greenhouse: (1) design and validation of a bes model for a plastic-covered greenhouse considering the tomato crop model and natural ventilation characteristics. *Agriculture* 2022;12:903. [\[CrossRef\]](#)
- [22] Ali HB. *Mesure et Modelisation des Bilans d'Énergie et de Masse (Eau) sur des Plantes Cultivées sous Serre: Impact d'une Restriction Hydrique*. (Dissertation Thesis). Angers; 24 Nov 2016.
- [23] Launder BE, Spalding DB. The numerical computation of turbulent flows. In: *Numerical Prediction of Flow, Heat Transfer, Turbulence and Combustion*. 1983. p. 96–116. [\[CrossRef\]](#)
- [24] Teitel M, Ziskind G, Liran O, Dubovsky V, Letan R. Effect of wind direction on greenhouse ventilation rate, airflow patterns and temperature distributions. *Biosyst Eng* 2008;101:351–369. [\[CrossRef\]](#)
- [25] Ali HB, Bournet PE, Cannavo P, Chantoiseau E. Using CFD to Improve the Irrigation Strategy for Growing Ornamental Plants Inside a Greenhouse. *Biosystems Engineering*. 2019;186:130–145. [\[CrossRef\]](#)

-
- [26] He X, Wang J, Guo S, Zhang J, Wei B, Sun J, Shu S. Ventilation Optimization of Solar Greenhouse with Removable Back Walls Based on CFD. *Comput Electron Agric* 2018;149:16–25. [\[CrossRef\]](#)
- [27] Tigampo S, Sambou V, Dieye Y, Toure PM, Bodian S. Study of air movement and temperature distribution in a greenhouse used as a dryer. *MATEC Web of Confer* 2020;307:01051. [\[CrossRef\]](#)
- [28] Kim K, Yoon JY, Kwon HJ, Han JH, Son JE, Nam SW, Giacomelli GA, Lee IB. 3-D CFD Analysis of relative humidity distribution in greenhouse with a fog cooling system and refrigerative dehumidifiers. *Biosyst Eng* 2008;100:245–255. [\[CrossRef\]](#)
- [29] ANSYS Fluent Inc. ANSYS Fluent Theory Guide. Pennsylvania, USA: ANSYS Fluent Inc; 2011.
- [30] Ali HB, Bournet PE, Cannavo P, Chantoiseau E. Development of a CFD crop submodel for simulating microclimate and transpiration of ornamental plants grown in a greenhouse under water Restriction. *Comput Electron Agric* 2018;149:20–40. [\[CrossRef\]](#)
- [31] Fatnassi H, Boulard T, Bouirden L. Simulation of climatic conditions in full-scale greenhouse fitted with insect-proof screens. *Agric Forest Meteorol* 2003;118:97–111. [\[CrossRef\]](#)
- [32] Villagran EA, Baeza Romero EJ, Bojaca CR. Transient CFD analysis of the natural ventilation of three types of greenhouses used for agricultural production in a tropical mountain climate. *Biosyst Eng* 2019;188:288–304. [\[CrossRef\]](#)